CeB_6 electron gun for low-emittance injector

K. Togawa,* T. Shintake, T. Inagaki, K. Onoe,† and T. Tanaka
RIKEN SPring-8 Center, 1-1-1 Kouto, Sayo, Hyogo 679-5148, Japan‡

H. Baba and H. Matsumoto
High Energy Accelerator Research Organization (KEK), 1-1 Oho, Tsukuba, Ibaraki 305-5148, Japan
(Received 6 December 2006; published 2 February 2007)

A high-voltage pulsed electron gun has been developed for the low-emittance injector system of the x-ray free electron laser (FEL) project at SPring-8. A single-crystal CeB_6 cathode was chosen as a thermionic emitter because of its excellent emission properties, i.e., smooth surface, high emission density, uniform emission density, and high resistance to contamination. A gun voltage of -500 kV was determined as a compromise between the need for suppressing emittance growth and reducing the risks of high-voltage arcing. We have succeeded in producing a 500 keV beam with 1 A peak current and 3 μs width. We have also measured the beam emittance by means of the double-slit method and obtained an extremely low emittance of 1.1π mm mrad (normalized, rms). These results are very promising for the x-ray FEL. In this paper, we describe the design and basic performance of the CeB_6 electron gun, and report the emittance measurement experiments.

DOI: 10.1103/PhysRevSTAB.10.020703 PACS numbers: 29.25.Bx, 41.60.Cr, 52.59.Mv, 79.40.+z

I. INTRODUCTION

Nowadays, the generation of a low-emittance high-intensity electron beam is an indispensable and key technology for future electron accelerators, e.g., x-ray free electron lasers (FEL), energy recovery linacs, and e^+e^- linear colliders. In the case of the x-ray FEL based on the process of self-amplified spontaneous emission (SASE), it is well known that the fine structure of the beam dominates the FEL gain. To achieve the gain saturation of SASE-FEL in the Angstrom wavelength region, the sliced emittance of the beam should be very low and the peak current should be of the order of kA. Moreover, from the application point of view, the FEL machine should be stable for long periods of operation.

In the x-ray FEL, the electron beam generated by the gun is accelerated in the main linac; then, it is directly injected into the long undulator and an x-ray beam is generated there. Therefore, any fluctuations of the electron bunch in the transverse position, timing, size, charge, etc. will directly affect the x-ray lasing. This is markedly different from the case of the storage-ring-type machine. As a result, stability of the electron gun is essential for producing a stable x-ray FEL light.

In the SPring-8 Compact SASE Source (SCSS) project, we decided to use a thermionic cathode followed by a buncher system [1–3]. This is a conventional injector system used in many types of electron accelerators. High stability and long lifetimes have been routinely achieved in present-day injectors; however, for these conventional applications, the typical emittance is $\sim 30\pi$ mm mrad or larger. In order to reduce the emittance, we have made the following modifications and upgrades.

(i) Small-size cathode.—The initial emittance of the gun is dominated by its cathode size. We use a single-crystal CeB_6 cathode with a 3 mm diameter. The theoretical thermal emittance is 0.4π mm mrad at $\sim 1400\,^\circ$C. A high beam current of ≥ 1 A can be produced from the CeB_6 crystal at this temperature without jeopardizing its long lifetime.

(ii) Elimination of the cathode control grid.—The emittance of the traditional thermionic cathode gun is degraded by the electric field distortion caused by the grid mesh.

(iii) Application of 500 kV to the cathode.—In order to minimize emittance growth due to space-charge effects, a higher gun voltage is desirable. We use a 500 kV pulse with a width of only a few microseconds.

(iv) Fast beam deflector.—To form a nanosecond single-electron bunch from the long pulse generated by the gun, we use a fast-pulsed beam deflector after the gun. Since an unused part of the long-pulsed beam is bent to a beam dump, this system is free from a cathode-dark-current, which prevents us from fine-beam-tuning and causes radiation damage to the undulator magnets.

(v) Adiabatic bunching and acceleration.—In order to minimize emittance growth due to the rf field, a lower rf frequency is desirable. We use a 238 MHz subharmonic buncher, followed by a 1.6 m drift section, and then a 476 MHz booster cavity that raises the beam energy up to 1 MeV. An L-band pre-linac following the booster cavity is used to capture and accelerate the electron bunch to ~ 40 MeV before its injection into the accelerating section composed of an S-band pre-linac, bunch compressors, and a C-band main linac.

*Electronic address: togawa@spring8.or.jp
†Present address: ULVAC TECHNO, Ltd., 2609-5 Hagizono, Chigasaki, Kanagawa 253-8555, Japan.
‡URL: http://www-xfel.spring8.or.jp/

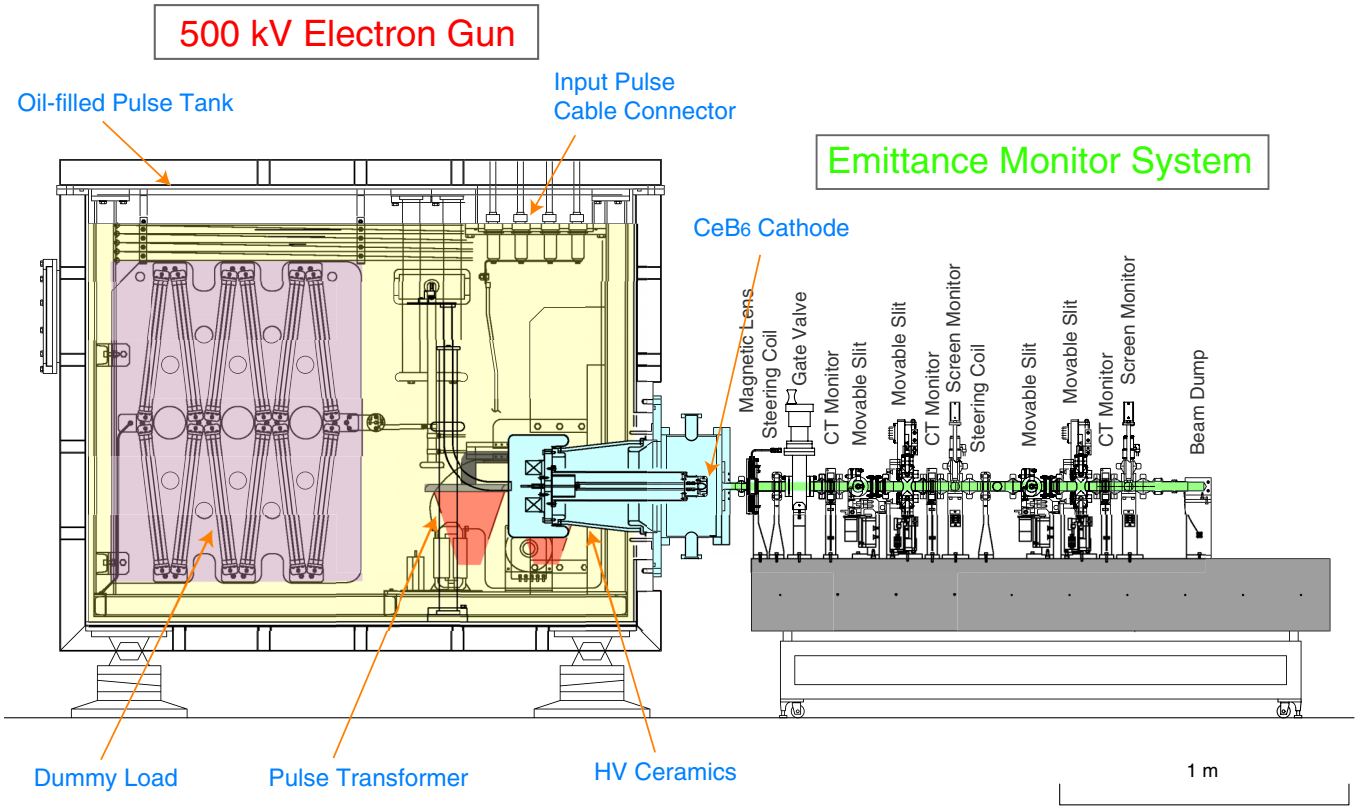

FIG. 1. (Color) Side view of the CeB_6 electron gun with an emittance monitor bench.

In this paper, the design details and basic performance of the CeB_6 electron gun are described, and the emittance measurement experiments are reported.

II. THE CeB_6 GUN

A side view of the CeB_6 electron gun with an emittance monitor bench is shown in Fig. 1, and the beam design parameters at the gun exit are summarized in Table I.

A. CeB_6 cathode

The normalized rms thermal emittance of electrons emitted from a hot cathode can be described as

$$\varepsilon_{n,\mathrm{rms}}^{\mathrm{th}} = \frac{r_c}{2}\sqrt{\frac{k_B T}{m_e c^2}},$$

where r_c is the cathode radius, k_B is Boltzmann's constant, and T is the cathode temperature. From the above relation, in order to obtain a small emittance of less than 1π mm mrad that is required for the x-ray FEL, the cathode diameter must be in the range of a few mm and should be in the temperature range of 1000–1500 °C. On the other hand, a high emission density ($\gtrsim 30$ A/cm^2) is required to produce a peak current of several amperes from the small surface of the cathode. Rare-earth hexaborides such as LaB_6 or CeB_6 can emit such an intense current over long lifetimes. A single crystal is preferable for obtaining low emittance because of its extremely flat surface (roughness of ≤ 1 μm) and low porosity after surface material evaporation [4]. The emission density is more uniform because the crystal orientation is constant over the whole surface. In recent years, single-crystal CeB_6 cathodes have been widely used for electron microscopes and superior stability has been demonstrated [5]. It is reported that CeB_6 is very resistant to carbon contamination as compared with LaB_6. Moreover, the operational temperature of CeB_6 can be lower than that of LaB_6 because of its lower work function (~ 2.4 eV).

For the above reasons, we decided to use a single-crystal CeB_6 cathode with a [100] crystal face. The diameter of our CeB_6 cathode is 3 mm. More than 1 A peak current is produced when the cathode is heated to $\gtrsim 1400$ °C. The theoretical thermal emittance is 0.4π mm mrad.

Figure 2 shows the CeB_6 crystal, the cathode being heated in the test chamber, and the cross-sectional drawing

TABLE I. Beam design parameters at the gun exit.

Beam energy	500 keV
Peak current	1–3 A
Pulse width (FWHM)	1.6 μs
Repetition rate	60 Hz
Normalized emittance (rms)	0.4π mm mrad

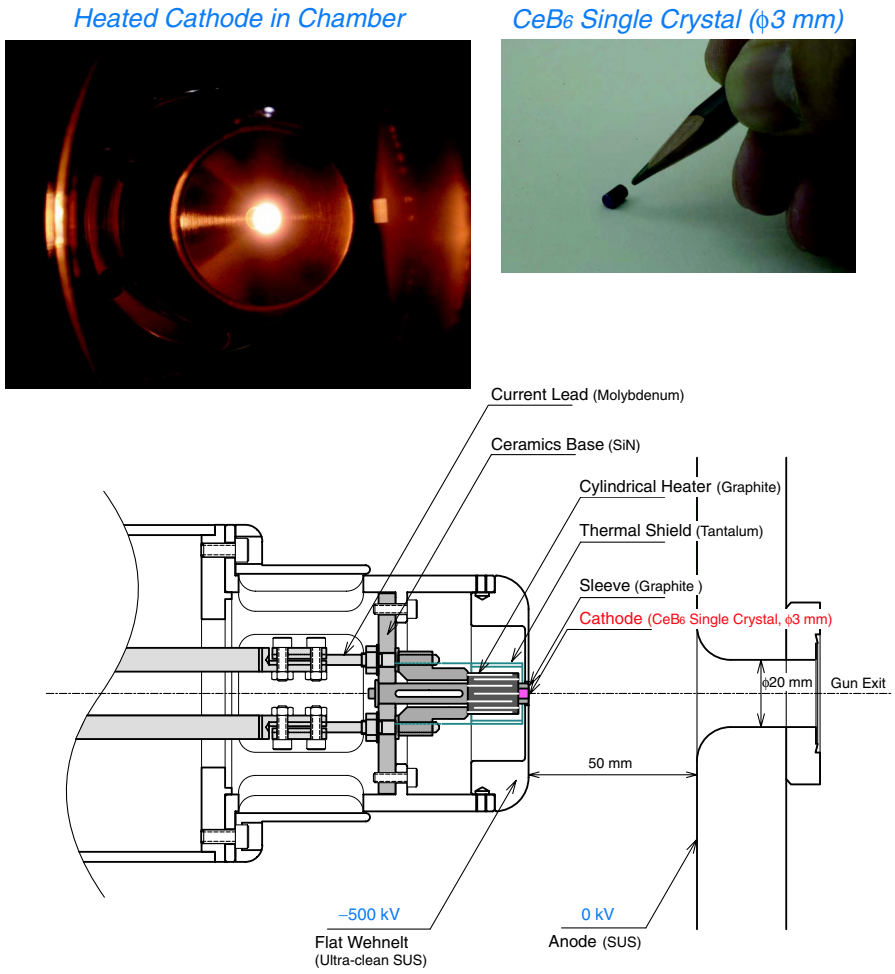

FIG. 2. (Color) CeB_6 cathode assembly.

of the cathode assembly with accelerating electrodes. The CeB_6 crystal is mounted in a graphite sleeve, which produces a uniform electric field over the entire cathode surface. This is quite important for the elimination of any beam emission halo coming from the cathode edge, which could cause damage to the undulator magnets.

We use a graphite heater instead of a conventional metallic filament made of tungsten or a similar metal; this is because graphite is mechanically and chemically stable even at very high temperatures and does not evaporate like other metals. Since its electrical resistance does not change significantly as a function of temperature, it is easy to control the heater power. The heater resistance is 0.18 Ω.

A tantalum cylinder covers the graphite heater to shield the thermal radiation from its surface. The base plate for the cathode assembly is made of silicone nitride, which is mechanically strong even when thermal stresses are applied.

The cathode was heated up to ∼1400 °C in the test chamber by applying 210 W of heater power (see the upper left side of Fig. 2). The reference temperature was measured at the graphite sleeve surrounding the cathode by means of a radiation monitor. The cathode was operated for more than 10 000 h without failure.

B. Accelerating electrode

The accelerating electrode was designed and manufactured carefully because it controls the initial condition of the emerging low-energy beam. We chose a flat Wehnelt electrode instead of the common Pierce-type electrode. The reasons for this are as follows: (i) The Pierce electrode was originally designed to produce a parallel beam whose space-charge field is balanced by a focusing electric field. However, if the cathode is not exactly centered due to a misalignment of the cathode mount or shifts in the cathode position caused by heating, an asymmetric focusing field acts on the beam, which may cause emittance growth. The flat Wehnelt electrode does not have such an effect. (ii) We planned to vary the beam current over a wide range in order to tune the accelerator system, and the gun would be operated in a temperature-limited region. The Pierce electrode is not suitable for such an operational mode; this is

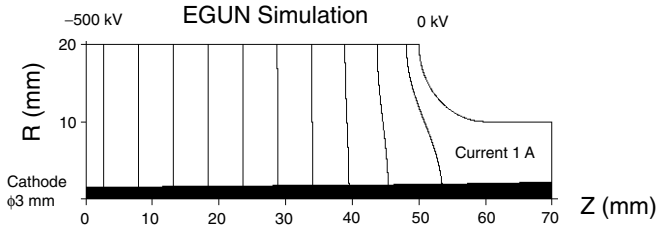

FIG. 3. Beam trajectory near the gun electrode.

because at a low current, the beam is overfocused, and the flat Wehnelt electrode does not overfocus the beam.

The space-charge limited current is described as

$$I_{scl} = \frac{4}{9}\epsilon_0\sqrt{\frac{2e}{m_e}}\frac{S}{d^2}V^{3/2}F,$$

where V is the gap voltage, d is the electrode gap distance, and S is the cathode area. In the case where the cathode radius is much smaller than d, the space-charge limited current becomes higher than that in the case of an infinite parallel electrode. In order to take this effect into account, we introduce an enhancement factor, F, into Child's law. By performing both an analytical evaluation and computer simulation, it was found that the enhancement factor is a function of r_c/d. After setting the gap distance d to be 50 mm, F becomes about 5 and the space-charge limited current becomes ~12 A [1]. The details are described in Appendix A. Since this current is much higher than the required current, the cathode will be operated in the temperature-limited region. In that case, the electric field near the cathode surface is higher than it would be in the space-charge limited region. Since the beam near the cathode is instantaneously accelerated, it is expected that the emittance degradation due to space-charge effects would be minimized.

We performed a computer simulation for a 500 keV, 1 A beam operation using the EGUN code [6]. As shown in Fig. 3, the beam does not diverge much in the electrode gap. When the calculated mesh size is set to a small value, the phase-space plot becomes a straight line and the emittance without initial thermal motion converges to less than 0.1π mm mrad for mesh sizes below 0.05 mm [7].

The maximum field on the Wehnelt edge is calculated to be 26 MV/m at 500 kV using the POISSON code [8]. The electrode is carefully manufactured to avoid breakdown discharge problems at this high field. Ultraclean stainless steel is used as the electrode material. Its surface was

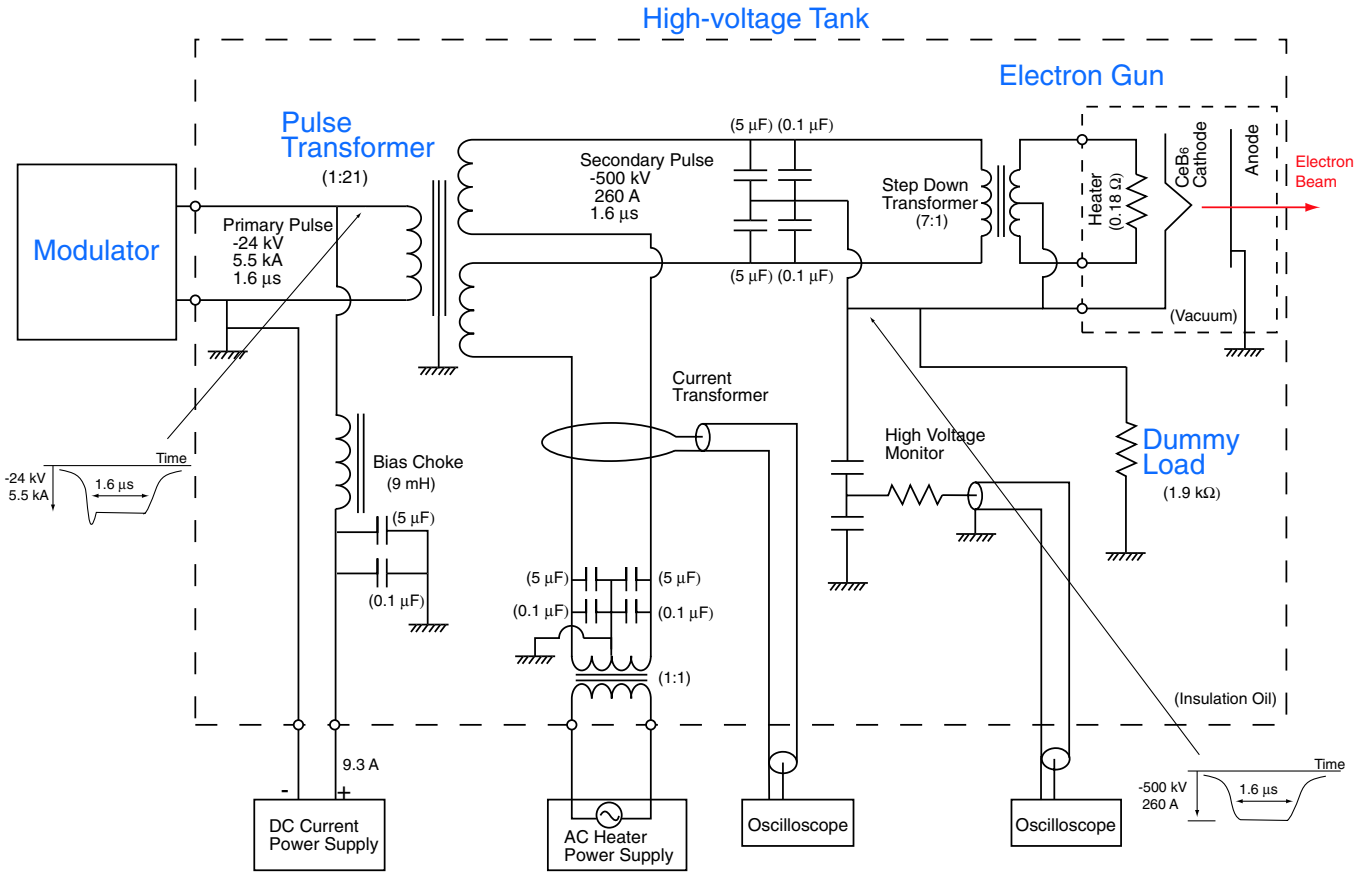

FIG. 4. (Color) Circuit diagram of the gun high-voltage tank.

chemically etched and rinsed with ultrapure water to remove any hydrocarbon contamination, which promotes discharges.

C. High-voltage tank

The circuit diagram for the high-voltage tank is shown in Fig. 4. It follows the design convention for a klystron tank. Nowadays, it is technically feasible to produce 500 kV pulses in high-power devices, such as X-band klystrons and high-voltage guns [9,10]. Therefore, we can use the same model of the C-band klystron modulator to feed a -24 kV pulsed voltage to the gun high-voltage tank [11]. The primary pulse is stepped-up to -500 kV by a pulse transformer with a turns ratio of 1:21. In order to match the impedance of the gun to the modulator pulse-forming-network output circuit, a 1.9 kΩ dummy load is connected in parallel with the cathode. AC power for the cathode heater is fed through the secondary winding of the pulse transformer. Since the heater current is very high (> 30 A), a step-down transformer, whose turns ratio is 7:1, is used to reduce the IR power loss in the transmission line from the power supply to the cathode.

Since we need to apply a -500 kV pulsed voltage to the cathode, all the high-voltage components, namely, the ceramic insulator, pulse transformer, dummy load, etc., are immersed in insulating oil to eliminate discharge problems. Before operation, the high-voltage tank is pumped out to eliminate the gases remaining in the oil and the high-voltage components.

Figure 5 shows the waveform of the gun voltage and beam current. The beam current was measured by a current transformer (CT) located in the beam line right after the gun. The beam energy is 500 keV, and the peak current is 1 A. The flattop portion of the pulse is about 0.8 μs, which is sufficient to generate a nanosecond electron bunch.

The high-voltage pulse width was observed to be 2 times longer than the design value; this long pulse duration was due to the fairly large stray capacitance of the dummy load resistors. As a result, the heat load to be removed from the high-voltage tank was higher than the design expectation. The large size of the high-voltage tank is also because of the resistors. Therefore, in order to shorten the pulse width and make the tank more compact, we have developed an electron tube dummy load, which replaced the load resistors [2]. The compact gun tank with the dummy tube has been constructed and is routinely operating in a 250 MeV prototype accelerator for the SCSS project.

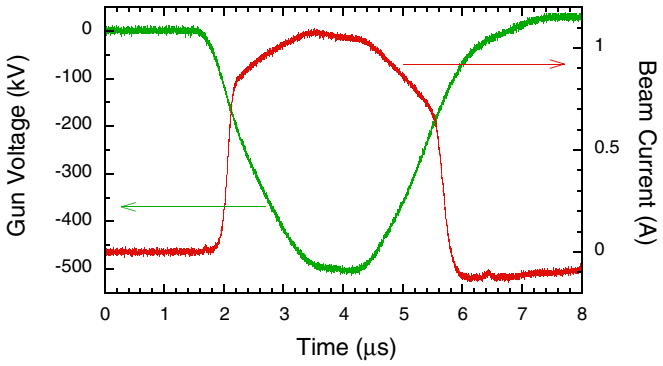

FIG. 5. (Color) Waveform of the gun voltage and beam current.

III. BEAM EMISSION PROPERTIES

The emission current density from a hot cathode is governed by Richardson's equation:

$$J = AT^2 \exp\left(-\frac{\phi_{\text{eff}}}{k_B T}\right), \qquad \phi_{\text{eff}} = \phi - \frac{e}{2}\sqrt{\frac{eE_s}{\pi\epsilon_0}},$$

where A is the Richardson constant (ideally, 120.4 A cm^{-2} K^{-2}), ϕ is the work function of the cathode material, ϕ_{eff} is the effective work function reduced by Schottky effect, and E_s is the electric field on the cathode surface. We have measured the emission current for various cathode temperatures at -500 kV and plotted the Richardson plot as shown in Fig. 6. The data fit well into Richardson's equation, and A of 19.1 A cm^{-2} K^{-2} and ϕ_{eff} of 2.26 V are obtained. Using E_s of 12.6 MV/m calculated by the POISSON code, ϕ is estimated to be 2.39 V. This is a reasonable value compared with the manufacturer's data [5]; however, the empirically obtained A is fairly smaller than the ideal value. In classical theory, A is determined only by fundamental physics constants; however, it is in fact strongly dependent on the materials used [12]. The mechanism that causes the discrepancy between the theo-

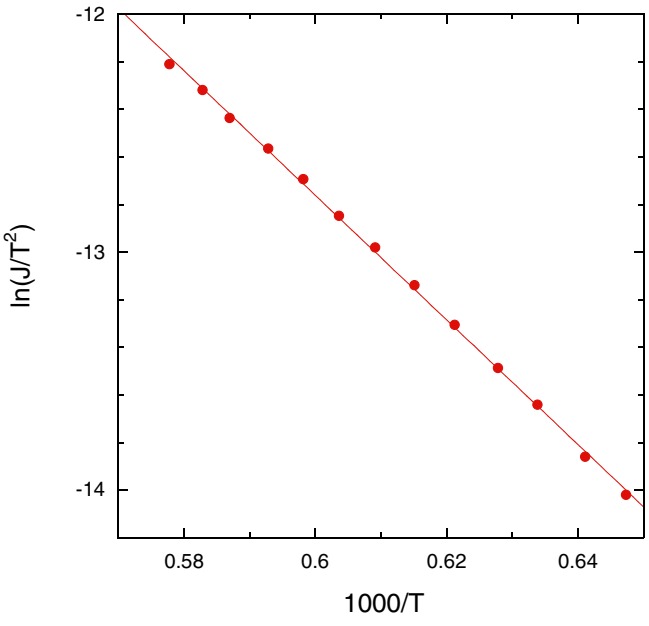

FIG. 6. (Color) Richardson plot for the CeB_6 cathode. Temperature T is expressed in Kelvin and current density J in A/cm^2.

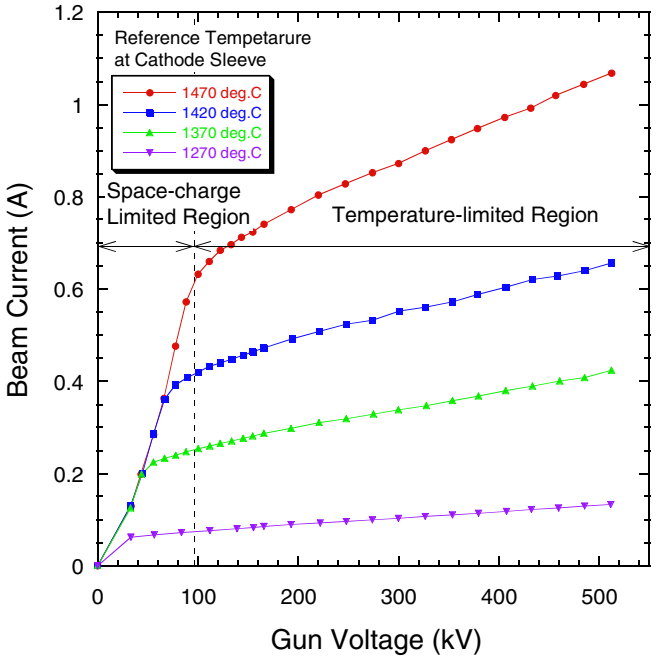

FIG. 7. (Color) Current-voltage characteristics of the CeB_6 gun.

retical Richardson constant and the empirical one is not clarified yet.

Figure 7 shows the current-voltage characteristics of the CeB_6 gun at various cathode temperatures. In the temperature-limited region, the beam current is dominated by the Schottky effect ($I \propto \exp\sqrt{V}$) rather than Child's law ($I \propto V^{3/2}$); that is, the slope of the current-voltage curve reduces. As a result, it is expected that the beam intensity jitter caused by the gun voltage jitter is suppressed. However, since the operational voltage exceeds the space-charge limited region, the beam current does not saturate any longer. If the beam-current fluctuation is caused by a change in the environment, e.g., vacuum pressure, oil temperature in the gun tank, or room temperature, we must precisely control the electric power fed to the cathode heater in order to stabilize the beam current.

IV. EMITTANCE MEASUREMENT

A. Double-slit method

We measured the beam emittance by the double-slit method [13]. A schematic diagram of the measurement principle is shown in Fig. 8. The upstream slit produces a sheet-shaped beamlet from the round beam, which spreads after passing through the drift space due to transverse thermal motion and space charge. The downstream slit measures the beamlet profile. By scanning both the slits throughout the beam area, the intensity profile of the beam in the phase space can be obtained. We prepared four slits, two for horizontal (x-direction) scan and two for vertical (y-direction) scan. The upstream x-slits were located 500 mm downstream from the cathode, followed by a

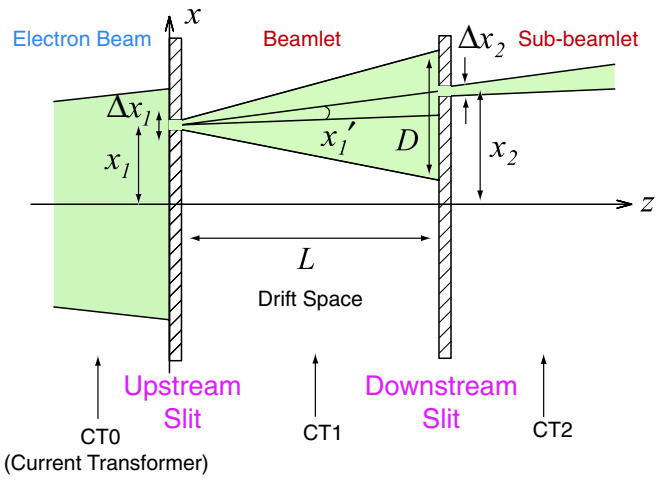

FIG. 8. (Color) Principle of emittance measurement. The vertical slits are omitted in the figure.

600 mm drift space (L) and the downstream slit. A solenoid lens, located 134 mm downstream from the cathode, was used to focus the beam to a proper size. The CT monitors measured the waveforms of the pulsed beam currents.

We observed that the combination of slits and CT monitors with a conventional digital scope is a very powerful tool to analyze the beam dynamics in the time domain. The sub-beamlet current waveform provides information on the time evolution of the phase-space intensity at a certain point. The time evolution of the phase-space profile can be reconstructed from about 1500 waveforms stored by the slit scan. Figure 9 shows an example of the animation screens of the phase-space profile evolution. Using a pair of vertical and horizontal slits, a time-resolved beam profile can also be measured by the same method.

The opening width must be narrow enough to ignore the beamlet broadening due to the space charge. Figure 10 shows the beamlet intensity profiles for several values of the upstream slit width Δx_1 (25, 50, 100, 200 μm). The original beam energy and current were 400 keV and 0.9 A, respectively. The downstream slit width Δx_2 was set to 25 μm; the accuracy of the width and position are better than 10 μm. The profile became a clear Gaussian profile for the narrow slit width of less than 100 μm, as expected from the mirrorlike flat surface of the single-crystal CeB_6 cathode.

We have measured the current density profile for the 500 keV beam with a 1 A peak current. Figure 11 shows the three-dimensional plot of the current density profile at a flattop portion of the 3 μs pulsed beam. The width of both the x and y slits was set to 0.5×0.5 mm, and the scan step was 0.5 mm. The profile shows a reasonably flattop shape, as expected from the cathode geometry. Figure 12 shows the two-dimensional plot of the phase-space profile (x-direction) measured for the same beam parameters. The width of both the upstream and downstream slits was set to 50 μm; the scan step was 0.25 mm for the upstream

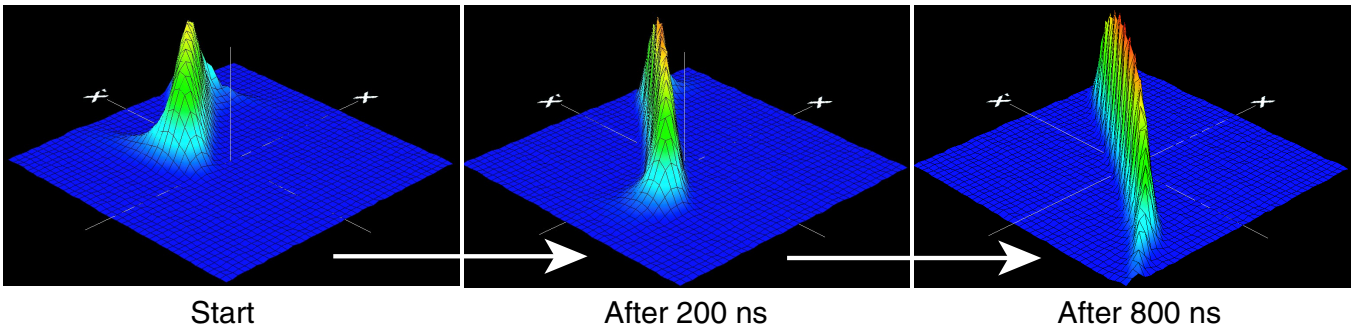

FIG. 9. (Color) Time evolution of the phase-space profile.

slit and 0.1 mm for the downstream slit. Almost all electrons distribute linearly and a smaller beam halo is observed on the screen.

B. Data analysis and discussion

From the phase-space profile, we analyzed the normalized rms emittance, defined as

$$\varepsilon_{n,\mathrm{rms}} = \beta\gamma\sqrt{\langle x^2\rangle\langle x'^2\rangle - \langle xx'\rangle^2},$$

where $\langle\,\rangle$ denotes the mean value weighted by the current density, β is the beam velocity divided by light velocity, and γ is the relativistic mass factor. The measurement of the rms emittance was very sensitive to background noise. The electric noise signal became a false increase in the emittance. In order to reduce the random noise generated by the A/D converter of the digital scope, each sub-beamlet current was determined by averaging 100 data values in the flattop region of the waveform. The noise level (3σ) that remained after the averaging was $\sim$1% of the peak intensity. To further reduce the noise influence, we analyzed the emittance using those data values that were greater than the noise level, and then we corrected it to the expected value without noise. As a result of this careful analysis, a normalized rms emittance of $1.10 \pm 0.08\pi$ mm mrad was obtained for the 500 keV, 1 A beam. The error consists of

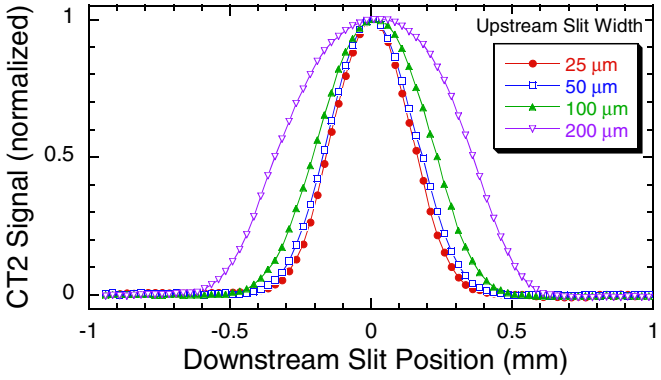

FIG. 10. (Color) Beamlet profiles for different upstream slit widths.

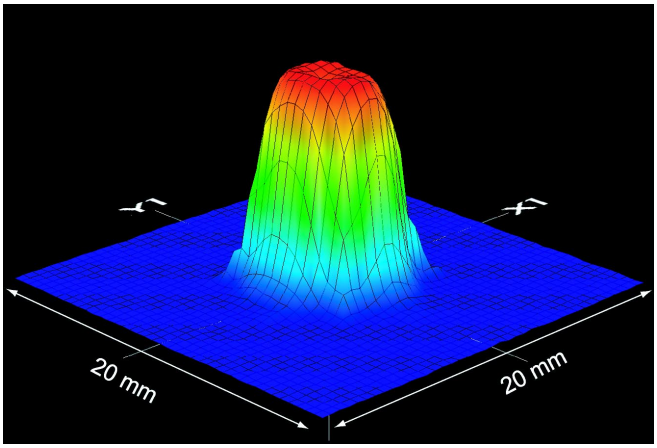

FIG. 11. (Color) Current density profile of the 500 keV, 1 A beam.

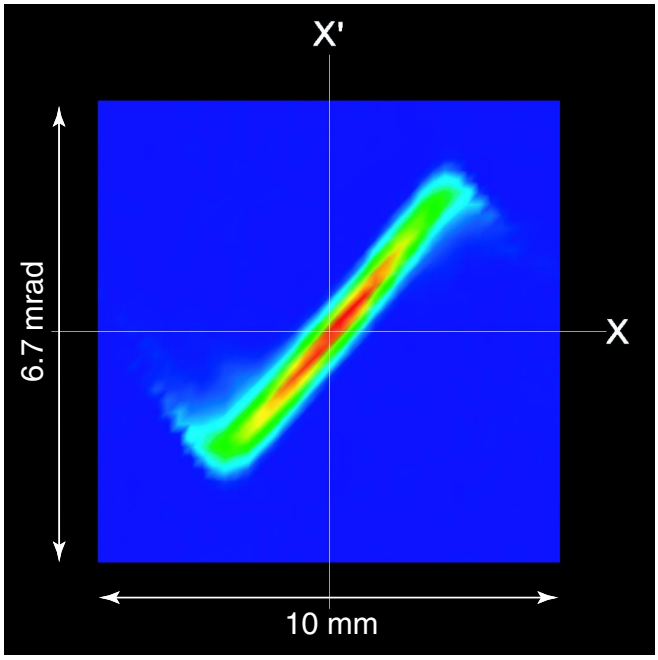

FIG. 12. (Color) Phase-space profile of the 500 keV, 1 A beam.

random error in the multiple measurements and the systematic error that originated in the gun voltage, the slit position, and the finite sampling number.

We achieved a very small emittance; however, it was slightly larger than the theoretically predicted value. A small tail at the profile edge is the source of the emittance increase, which may be generated by the space-charge effect.

The equation of motion of electrons in a space-charge dominated beam is described as

$$\frac{d^2r}{dz^2} = \frac{2I(r)}{I_0(\beta\gamma)^3}\frac{1}{r}, \qquad I(r) = \int_0^r J(r_1)2\pi r_1 dr_1,$$

where I_0 is the Alfvén current (17 kA) and $J(r)$ is the beam-current density at a radial position r. If the current density is uniform across the whole beam, i.e., if $J(r)$ is constant, the beam divergence dr/dz is proportional to the position r. In this case, the beam emittance does not increase due to the space charge. Since the emittance growth is related to the nonlinearity of dr/dz, the unnormalized emittance will vary as a function of $I/(\beta\gamma)^3$ [for the normalized emittance, $I/(\beta\gamma)^2$].

In order to investigate the space-charge effect on emittance, we have measured the emittance for beam energies from 250 to 500 keV and currents from 0.1 to 1 A. The measured emittance values are plotted as a function of $I/(\beta\gamma)^2$ in Fig. 13. It is clearly observed that the emittance growth becomes more pronounced at a lower energy and higher current. These data suggest that an unexpected nonlinear phase-space profile was formed at the emerging low-energy region near the cathode; then, the emittance grew by the nonlinear space-charge force in the electrode gap (50 mm) and drift space up to the upstream slit (450 mm).

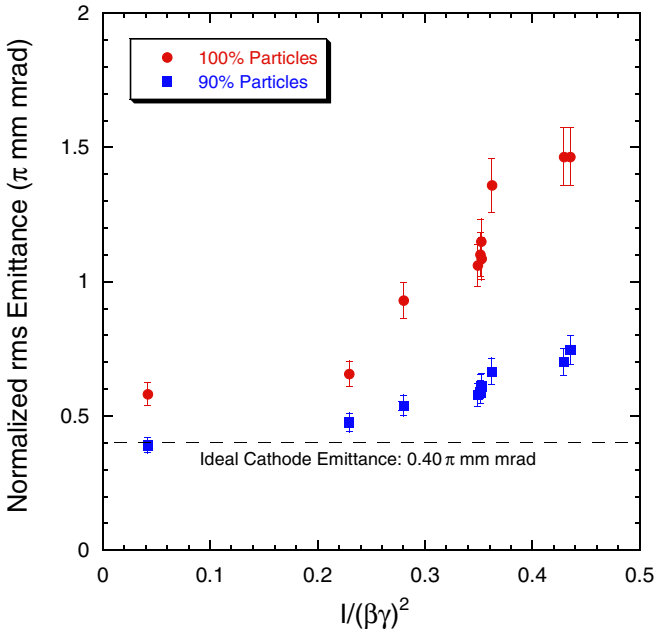

FIG. 13. (Color) Emittance growth as a function of normalized current, $I/(\beta\gamma)^2$.

TABLE II. Demonstrated beam parameters at gun exit.

Beam energy	500 keV
Peak current	1 A
Pulse width (FWHM)	3 μs
Repetition rate	10 Hz
Normalized emittance (rms, 100% electrons)	1.1π mm mrad
Normalized emittance (rms, 90% electrons)	0.6π mm mrad

Recently, the DESY group proposed a "core" emittance to evaluate beam quality; this is because the low intensity part of the phase-space profile does not contribute to x-ray lasing [14]. The core emittance is defined as the normalized rms emittance obtained using 90% of the electrons existing in the central region of the phase space. The core emittance values were measured and plotted in Fig. 13. The growth rate of the core emittance is much less than that of the full emittance. These data show that only 10% of the electrons cause the emittance growth, and the core emittance is close to the predicted thermal emittance.

Finally, the demonstrated beam parameters at the gun exit are summarized in Table II.

V. SUMMARY

To summarize, we have developed a 500 kV pulsed gun using a single-crystal CeB_6 cathode, and we successfully generated a high-intensity beam. We have also measured the beam emittance by means of the double-slit method, and we obtained a very small emittance of 1.1π mm mrad for the 500 keV, 1 A beam. A small tail at the profile edge, which may be generated by the space-charge effect, acts as a source of the emittance increase. However, the core emittance of 0.6π mm mrad is close to the theoretical thermal emittance. Since the nonlinear tail comes from the edge region of the round beam, it can be removed by using a beam collimator. We expect that by doing this, we can realize a small emittance of less than 1π mm mrad that is required for the x-ray FEL injector.

The CeB_6 gun is routinely operating and generating a 60 nm laser beam in the 250 MeV prototype accelerator [15,16]. We therefore conclude that the CeB_6 gun is very suitable for the low-emittance injector system of the x-ray FEL.

ACKNOWLEDGMENTS

We would like to thank the staff of Sumitomo Heavy Industries for constructing the 500 keV electron gun and emittance monitor bench. We also thank Dr. Ohata and the SPring-8 beam line control group members for developing the control system of the emittance monitor.

APPENDIX A: A MODEL OF SPACE-CHARGE LIMIT FOR FLAT ELECTRODES

The space-charge limit (SCL) of an electron gun current, which was found by Child in 1911 [17], is a one-dimensional theory. Therefore, it is suitable only for large-sized cathodes with flat-shaped electrodes. When the cathode size is considerably small compared with the electrode gap, the SCL becomes higher than that calculated using Child's law; this is because very little space charge exists between the Wehnelt cathode and anode. In this study, we developed a simple model of the SCL for the flat electrodes.

First, let us introduce the following three assumptions: (i) The beam does not spread in the radial direction by the space charge. (ii) Both the electric potential along the beam axis (z-axis) (ϕ) and the electric field on the cathode applied by the space charge (E_{sc}) do not depend on the radial position. (iii) When the beam current reaches the maximum limit, ϕ and E_{sc} become the same as those obtained from Child's law:

$$\phi = V\left(\frac{z}{d}\right)^{4/3}, \tag{A1}$$

$$E_{sc} = \frac{2V}{3d}, \tag{A2}$$

where V is the gap voltage and d is the electrode gap distance.

In the nonrelativistic case, the electron velocity is given by

$$v = \sqrt{\frac{2e\phi}{m_e}}. \tag{A3}$$

Using Eqs. (A1) and (A3), the space-charge density can be expressed as a function of z:

$$\rho = \frac{J}{v} = J\sqrt{\frac{m_e}{2eV}}d^{2/3}z^{-2/3}, \tag{A4}$$

where J is the current density. In addition, we assume that E_{sc} is given by integrating a central field from the disk charge at a position z. The central field is given by

$$dE = \frac{\rho dz}{2\epsilon_0}\left(1 - \frac{z}{\sqrt{z^2 + r_c^2}}\right), \tag{A5}$$

where dz and r_c are the thickness and radius of the disk charge, respectively (r_c also represents the cathode radius.) Substituting Eq. (A4) in Eq. (A5) and then integrating Eq. (A5), E_{sc} takes the following form:

$$E_{sc} = \int_0^d dE = \frac{J}{2\epsilon_0}\sqrt{\frac{m_e}{2eV}}d^{2/3}\int_0^d z^{-2/3}\left(1 - \frac{z}{\sqrt{z^2 + r_c^2}}\right)dz. \tag{A6}$$

From Eqs. (A2) and (A6), the space-charge limited current for a small cathode is obtained as

$$I_{scl} = \frac{4}{9}\epsilon_0\sqrt{\frac{2e}{m_e}}\frac{S}{d^2}V^{3/2}\frac{3d^{1/3}}{\int_0^d z^{-2/3}(1 - \frac{z}{\sqrt{z^2+r_c^2}})dz}, \tag{A7}$$

where S is the cathode area. Performing the change of variable, $z/d = x$, and using the limited current of Child's law (I_{Child}), I_{scl} can be expressed as

$$I_{scl} = I_{\mathrm{Child}}\left(1 - \frac{1}{3}\int_0^1 \frac{x^{1/3}}{\sqrt{x^2 + (r_c/d)^2}}dx\right)^{-1} = I_{\mathrm{Child}} \cdot F. \tag{A8}$$

The value F represents the enhancement factor of the space-charge limited current for the flat electrodes. It should be noted that F is a function of only the ratio of the cathode radius to the electrode gap (r_c/d). The numerically calculated F is shown in Fig. 14. For the purpose of comparison, some F values analyzed by the EGUN code and one experimental data value obtained from Fig. 7 are also plotted in that figure. At a low energy of less than 100 keV, the beam was collimated by the beam pipe just after the anode hole; thus, the experimental data for F data was corrected using the beam transfer efficiency from the cathode to the CT monitor, which was analyzed by the EGUN code. We can see that these F values have a tendency to increase near the origin and approach unity at a large r_c/d.

The numerically calculated F became somewhat lower than the experimental value and EGUN results at low r_c/d.

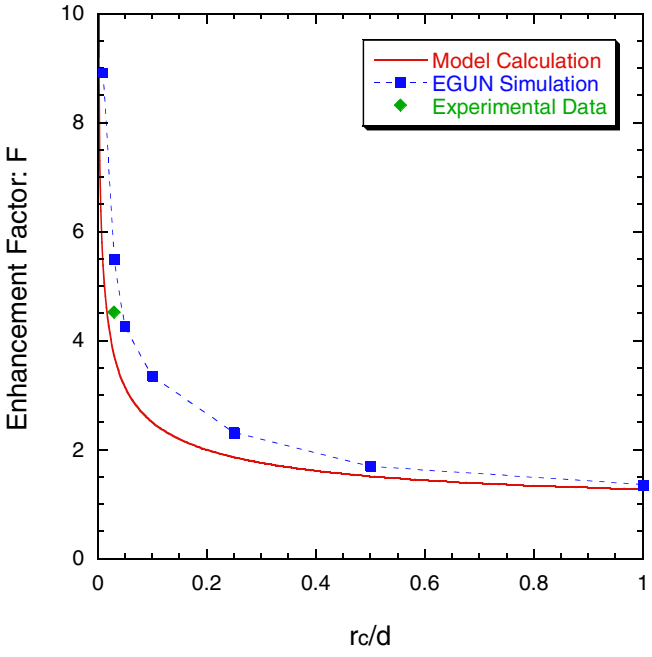

FIG. 14. (Color) Enhancement factor of space-charge limited current for flat electrodes as a function of the ratio of the cathode radius (r_c) to the electrode gap (d).

The first assumption in the model calculation seems to be the cause of this discrepancy. In the space-charge limited regime, the actual beam spreads considerably in the flat electrodes because there is no focusing electric field. Since the space-charge density decreases in this condition, the space-charge limited current becomes higher than that in the model calculation.

[1] T. Shintake, H. Matsumoto, T. Ishikawa, and H. Kitamura, in *Proceedings of SPIE, Optics for Fourth-Generation X-Ray Sources*, edited by R. O. Tatchyn, A. K. Freund, and T. Matsushita (SPIE, Bellingham, WA, 2001), Vol. 4500, pp. 12–23.

[2] SCSS X-FEL R&D Group, *SCSS X-FEL Conceptual Design Report*, edited by T. Shintake and T. Tanaka (RIKEN Harima Institute/SPring-8, Sayo, Japan, 2004).

[3] K. Togawa, H. Baba, K. Onoe, T. Inagaki, T. Shintake, and H. Matsumoto, Nucl. Instrum. Methods Phys. Res., Sect. A **528**, 312 (2004).

[4] H. Kobayashi, Y. Yamazaki, T. Kurihara, I. Sato, A. Asami, S. Otani, and Y. Ishizawa, in *1992 Linear Accelerator Conference Proceedings*, edited by C. R. Hoffmann (Chalk River Laboratories, Ottawa, Canada, 1992), Vol. 1, pp. 341–343.

[5] http://www.feibeamtech.com/.

[6] W. B. Hermannsfeldt, SLAC Report 331, 1988.

[7] D. Yeremian (private communication).

[8] M. T. Menzel and H. K. Stokes, LA-UR 87–115, Los Alamos National Laboratory, 1987.

[9] D. Sprehn, G. Caryotakis, E. Jongewaard, R. M. Phillips, and A. Vlieks, SLAC-PUB 8346, SLAC, 2000.

[10] J. Haimson, B. Mecklenburg, G. Stowell, and E. L. Wright, in *Proceedings of the 1997 Particle Accelerator Conference*, edited by M. Comyn, M. K. Craddock, M. Reiser, and J. Thomson (IEEE, Piscataway, NJ, 1998), pp. 2808–2810.

[11] T. Inagaki, H. Baba, T. Shintake, K. Togawa, K. Onoe, H. Matsumoto, T. Takashima, and A. Tokuchi, in *Proceedings of APAC2004*, edited by J. Choi (Pohang Accelerator Laboratory, Pohang, Korea, 2005), pp. 654–656.

[12] J. M. Lafferty, J. Appl. Phys. **22**, 299 (1951).

[13] C. Lejeune and J. Aubert, in *Applied Charged Particle Optics*, edited by A. Septier, Advances in Electronics and Electron Physics Supplement 13A (Academic Press, San Diego, 1980), pp. 159–259.

[14] V. Miltchev, in *Proceedings of the 27th International Free Electron Laser Conference*, edited by D. H.-D. Nuhn (SLAC, Menlo Park, CA, 2005), pp. 556–559.

[15] T. Shintake and SCSS Group, Status of the SCSS Test Accelerator and XFEL Project in Japan, 10th biennial European Particle Accelerator Conference (EAPC'06), Edinburgh, UK, 2006.

[16] H. Tanaka, K. Togawa, H. Baba, T. Hara, A. Higashiya, T. Inagaki, H. Maesaka, H. Matsumoto, K. Onoe, Y. Otake, K. Shirasawa, T. Tanaka, T. Tanikawa, M. Yabashi, and T. Shintake, in *Proceedings of FEL2006* (BESSY, Berlin, Germany, 2006), pp. 769–776.

[17] C. D. Child, Phys. Rev. (Series I) **32**, 492 (1911).